Composite Structures 160 (2017) 300–311

Contents lists available at ScienceDirect

Composite Structures

journal homepage: www.elsevier.com/locate/compstruct

Fiber reinforced elastomeric isolators for the seismic isolation of bridges

Yasser M. Al-Anany *, Michael J. Tait

Dept. of Civil Engineering, McMaster Univ., 1280 Main St. West, Hamilton, ON L8S 4L7, Canada

ARTICLE INFO

Article history:
Received 17 June 2016
Revised 8 September 2016
Accepted 4 October 2016
Available online 5 October 2016

Keywords:
Seismic isolation
Bridge structures
Fiber-reinforced
Elastomeric isolator
Experimental testing
Finite element analysis

ABSTRACT

Unbonded fiber reinforced elastomeric isolators (U-FREI) have been proposed as a viable alternative to traditional steel reinforced elastomeric isolators (SREI) for use in low-rise building base isolation systems. The viability of U-FREI for this particular application was confirmed through an extensive evaluation of their lateral response under the condition of no rotational deformations of the loading supports. In order to extend the use of U-FREI to bridge applications the consideration of rotational deformation in the analysis is necessary as it is an important component in bridge isolator design. Currently, no data exists in the literature for investigating the influence of rotational deformation on the lateral response of U-FREI, to the best of authors' knowledge. Accordingly, an experimental and numerical study was completed on U-FREI to investigate their lateral behaviour under a range of vertical loads and rotational deformations in order to determine their suitability as a seismic isolator for bridges. The lateral stiffness and damping were computed experimentally for different levels of vertical pressure, angles of rotations and lateral deformations. Additionally, the resulting stress and strain state within the isolators under peak deformations was also evaluated numerically via 3D modelling and presented in this study.

1. Introduction

Earthquakes are one of the most devastating types of natural disasters, which often result in loss of life, a large number of structural failures, and significant socio-economic costs. As it is not possible to prevent earthquakes from occurring, designers must focus on mitigating their effects. This can be accomplished by either increasing the capacity/ductility of the structure or decreasing the seismic demand placed on the structure. While increasing the capacity/ductility of a structure has traditionally been the approach employed, it is not always the most effective [1]. Alternatively, decreasing the seismic demand placed on the structure can be achieved through base isolation, and is considered to be one of the most effective methods to reduce seismic induced damage [2].

Base isolation in bridge applications can be achieved by introducing low lateral stiffness elements, which are able to adequately support the vertical loads, between the superstructure (i.e. deck/girder) and substructure (i.e. pier/ abutments) as shown in Fig. 1. When these flexible elements are used to accommodate non-seismic induced rotations and lateral deformations experienced by the girders, they are typically referred to as bearings. However, they are often referred to as isolators when employed to reduce and redistribute seismic induced lateral forces (i.e. seismic isolation). Their low lateral stiffness shifts the period of the structure into the displacement sensitive region, where the resulting inertial forces are significantly reduced. This results in a reduction in the seismic demand on the structural elements.

The loading demands on bridge bearings have increased due to continued developments in bridge design, such as the introduction of frames with much larger spans and innovative forms (ex. curved and skewed girders) [3]. In order to handle this increase, improvements to existing bearing types and the development of new bearings types are needed. Consequently, recent research efforts have focused on replacing conventional isolators with more innovative types that can accommodate larger loads and deformations [4].

There are two primary types of seismic isolators: (1) sliding and (2) elastomeric [5]. The sliding isolation system is based on the transmission of lower shear forces to the structure through a medium with a low friction coefficient that is placed between the structure and its foundation. Sliding isolators are typically either pure friction isolators or friction pendulum isolators [6]. Elastomeric isolators, which have the combination of high stiffness in the vertical direction as well as rotational and horizontal flexibility, are among the most widely used type of seismic isolator. Elastomeric isolators are reinforced with steel plates, which result in a high vertical stiffness by limiting the bulging in elastomer layers. They are typically divided into three isolator types: low-damping

* Corresponding author.
E-mail addresses: alananym@mcmaster.ca (Y.M. Al-Anany), taitm@mcmaster.ca (M.J. Tait).

http://dx.doi.org/10.1016/j.compstruct.2016.10.008
0263-8223/

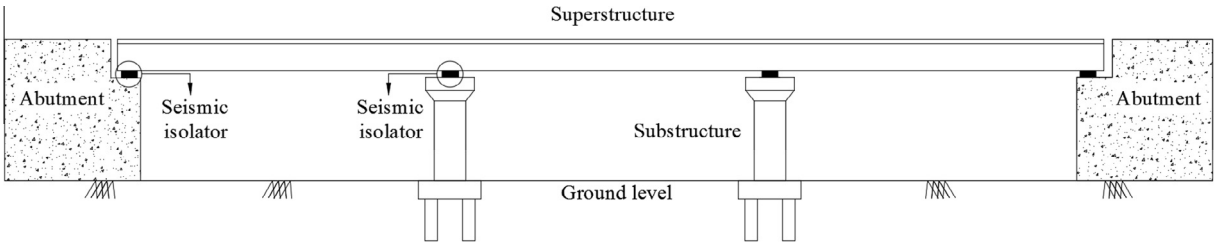

Fig. 1. Typical seismically isolated bridge.

natural rubber (LDR) isolators, lead-plug rubber (LPR) isolators and high-damping natural rubber (HDR) isolators [2].

A significant amount of research had been carried out to investigate the effectiveness of the aforementioned isolators (i.e. sliding and elastomeric) for the seismic isolation of bridges. Tsopelas [7,8] investigated the ability of sliding isolation systems to significantly reduce the seismic force transmitted to a bridge during a seismic event. Ghobarah and Ali [9] studied the effectiveness of LPR isolators for the seismic isolation of a typical three span highway bridge. Wesolowsky and Wilson [10] showed that isolators can decrease the accelerations and forces in cable-stayed bridges, which usually exhibit long natural periods due to their flexible cable-superstructure systems. Matsagar and Jangid [11] conducted a comparative numerical study on the seismic response of bridges isolated by friction pendulum, LDR and LPR isolators, and it was found that the seismic response of base-isolated bridges was highly influenced by the type and properties of the isolator employed. Jangid [1] evaluated the effect of using LPR isolators on the bidirectional seismic behaviour of bridges, and it was noted that neglecting the bidirectional interaction of LRP isolator restoring forces would result an underestimation in the isolator displacements.

2. Background

When fiber is used as the reinforcement for elastomeric isolators as a replacement for steel, the isolators are called Fiber Reinforced Elastomeric Isolators (FREI). FREI have potential advantages over traditional steel reinforced elastomeric isolators, including reduced manufacturing costs [12], increased corrosion resistance, and lower stress demand on the bond between the reinforcement and elastomer [13,14]. Moreover, in addition to the intrinsic damping of the elastomer, another source of energy dissipation is also provided via the interaction between the individual fibers within the fiber reinforcement layers [15,16].

Fiber reinforced elastomeric isolators can be unbonded (U-FREI), partially bonded (PB-FREI) or bonded (B-FREI) to both the superstructure and substructure. The variation in the deformation patterns between the unbonded and bonded isolator types can be observed in Figs. 2 and 3, respectively. An unbonded isolator experiences *rollover* when displaced laterally (see Fig. 2a), and *lift off* under excessive rotational deformations (see Fig. 2b). These deformation patterns (i.e. rollover and lift off) occur due to the lack of flexural rigidity provided by the fiber fabric reinforcement and also because of the unbonded boundary conditions. It can be observed from Fig. 3 that different deformation patterns occur if the isolator is bonded to the upper and lower platens. In general, unbonded isolators possess unique advantages over traditional bonded isolators under large lateral deformations [17] and large rotational deformations [18,19], such as:

i. Higher seismic isolation efficiency due to the significant reduction in lateral stiffness due to lateral rollover.
ii. Lower compressive stress demand on elastomer material as well as lower tensile stress demand on the fiber reinforcement.
iii. Reduced peeling stress demand on the bond between rubber and the fiber reinforcement layers as a result of the significant reduction in the shear strain demand.

A recent experimental research study by Al-Anany and Tait [20] found that U-FREI are capable of resisting large vertical loads and can accommodate lateral and rotational deformations under different loading scenarios that a bridge bearing is expected to experience over its design lifespan. Furthermore, no damage/delamination of the isolators was observed during the experimental study. However, the influence of rotational loads/deformations on the lateral response of U-FREI has not been investigated to date. The behaviour of U-FREI under such combined deformations must be determined in order to extend its utilizations to the seismic isolation of bridges. As such, the objective of this study is to investigate the lateral behaviour of U-FREI under a range of different rotational deformation amplitudes and vertical loads. The first section of this paper reports on the experimentally evaluated lateral response of U-FREI both with and without rotational deformations, including the effects of vertical loads and isolator aspect ratio. The second section describes the findings from a three-dimensional finite element (FE) analysis, including the resulting stress and strain state of the experimentally tested isolators.

3. Experimental program

3.1. Isolators specimens

A total of three quarter-scale U-FREI test specimens, having different geometric properties as shown in Table 1, were constructed and tested in the Applied Dynamics Laboratory (ADL) at McMaster University. Each specimen consisted of layers of natural rubber elastomer reinforced with bi-directional plain weave carbon fiber fabric. The intermediate elastomer layers had a thickness that was twice as large as the outer most elastomeric layers, which served as the top and bottom covers. All three isolators were cut from a single fiber-reinforced elastomeric pad with dimensions of $140 \times 140 \times 20.6$ mm (shown in Fig. 4).

In general, the behaviour of a U-FREI is predominantly influenced by its shape factor, S, and aspect ratio, AR. Both of these parameters must be properly selected in order to attain sufficient vertical and rotational stiffness [18,19] and maintain a stable response under different levels of lateral deformation [13,14,21]. The aspect ratio, which has a significant effect on the lateral response of a U-FREI, is defined as ratio between the total length/width and the total thickness of the isolator. The shape factor, which is the dominant parameter affecting the vertical response, is defined as the ratio between loaded area and the area free to bulge. The in plane dimension (direction of lateral testing) was varied, as shown in Table 1, in order to investigate the behaviour

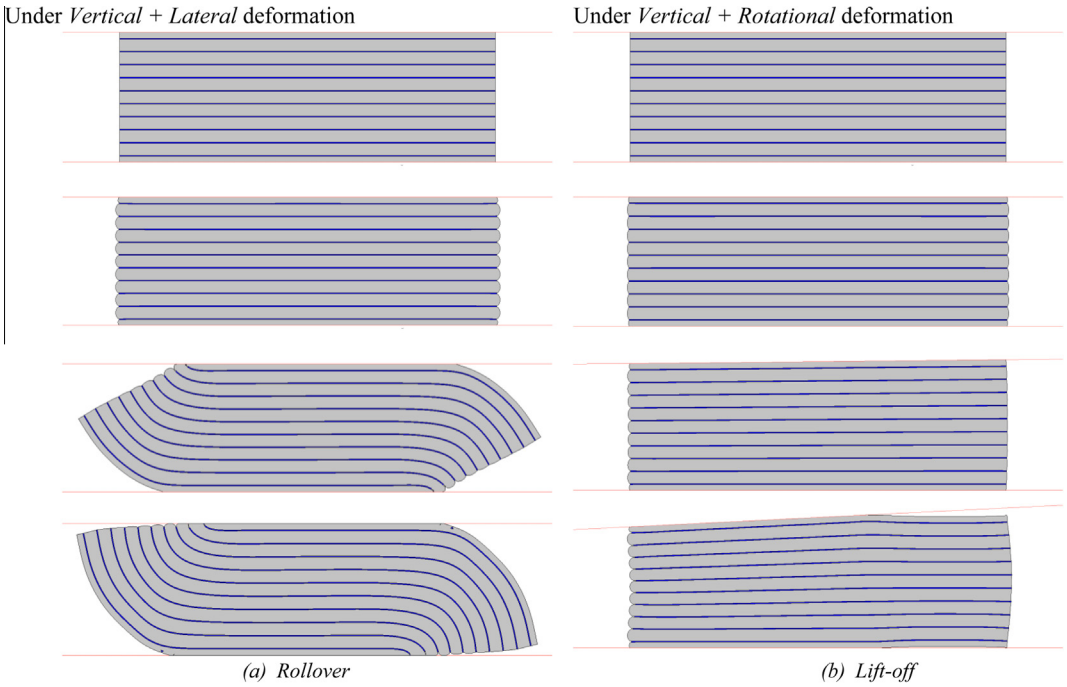

Fig. 2. Deformation patterns of U-FREI (i.e. unbonded).

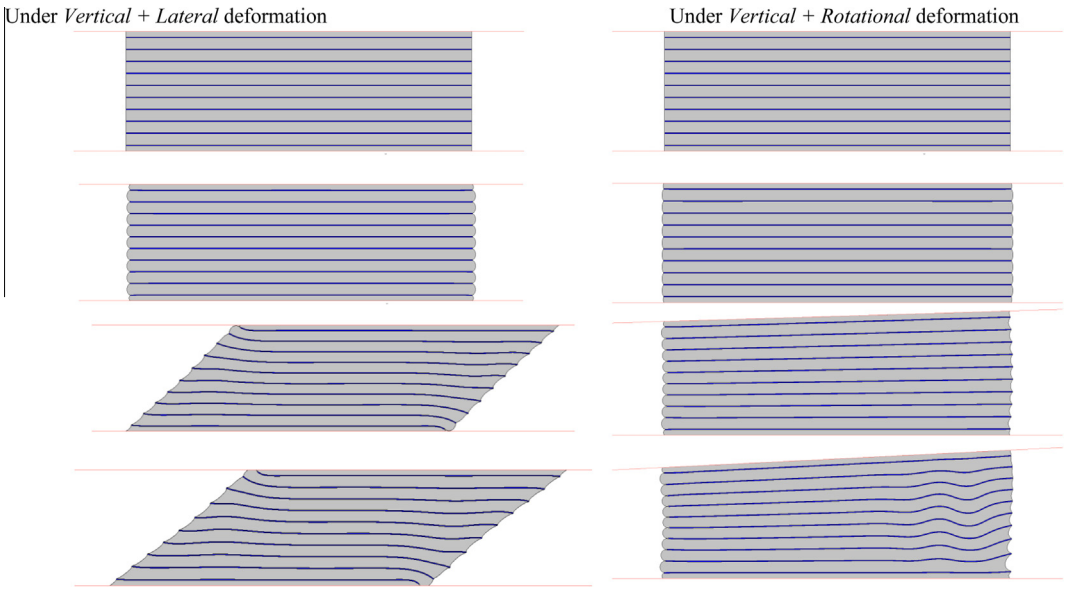

Fig. 3. Deformation patterns of B-FREI (i.e. bonded).

of U-FREI having aspect ratios of 2.5, 3.5, and 4.5. In addition, the out of plane dimension of all three isolators were also varied in order to maintain a constant shape factor value of 6.0. A shape factor of 6.0 falls within the range of typical values used in bridges applications (i.e. $3 < S < 8$) [22].

3.2. Test apparatus

A three-degree of freedom test apparatus was used to carry out the experimental testing, as shown in Fig. 5. The main components of the test apparatus include the loading beam, pedestal, and reaction frame as shown in Fig. 6. Three hydraulic actuators (2 vertical + 1 lateral), denoted as 1, 2, and 3 (see Fig. 6), were used to apply vertical, rotational, and lateral deformations on the test specimen. The vertical pressure (i.e. vertical loads) was applied under load control while both the lateral and rotational deformations (i.e. angles of rotational) were applied under displacement control.

3.3. Test program

In order to investigate the influence of static rotation on the lateral behaviour their response under different levels of rotational deformation were studied a total of 27 experimental tests were conducted on the U-FREI specimens. The parameters varied during the application of cyclic lateral displacements were the vertical load (P) and the static rotation (θ). Different levels of vertical load

Table 1
Geometric properties of the test specimen (all units are in mm).

	Isolator 1	Isolator 2	Isolator 3
Elastomer thickness (cover layers)	1.5	1.5	1.5
Elastomer thickness (intermediate layers)	3.0	3.0	3.0
Number of intermediate elastomer layers	5.0	5.0	5.0
Total elastomer thickness (t_r)	18.0	18.0	18.0
Fiber layer thickness	0.25	0.25	0.25
Number of fiber layers	6	6	6
Total fiber thickness	1.5	1.5	1.5
Total height of bearing (h)	19.5	19.5	19.5
Length ($2b$)	87.75	68.25	48.75
Width (a)	61.2	76.2	138.0
Aspect ratio (R) = $2b/h$	4.5	3.5	2.5
Shape factor	6	6	6

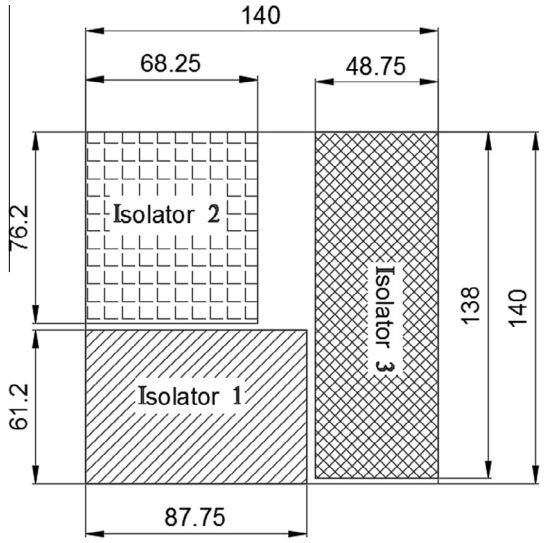

Fig. 4. Sketch of the original pad before cutting the isolators (all dimensions are in mm).

Fig. 5. Photograph of the three-degree of freedom test apparatus.

were applied in order to reach corresponding mean vertical compressive stresses (ratio between vertical load and the isolator plan area), σ_v, of 2.0, 6.0, and 10.0 MPa under pure compression. The values of applied static rotations were 0, 0.015, 0.03 rad.

The loading procedure used in this part of the study is shown in Fig. 7. The isolator was first loaded monotonically up to the target vertical load level. The top-loading beam was then rotated until the required value of static rotation was reached. Next, a total of 12 lateral cycles representing four different lateral amplitudes of magnitude 0.25, 0.50, 1.00, and 1.50 t_r were applied parallel to the specimen length ($2L$) at a lateral loading rate of 76 mm/s. Finally, the isolator was unloaded (monotonically) and the isolator was removed from test apparatus and visually inspected for damage.

4. Experimental program – results and discussion

Fig. 8 shows the lateral load–displacement response (hysteresis loops) of the isolators under different vertical pressures and applied rotations. The loops are normalized per unit width of the isolator and elastomer shear modulus (G_e) value of 0.86 MPa, which was calculated based on the average experimental results of the three isolators. It can be observed from Fig. 8 that all the isolators maintained a stable rollover response (i.e. tangential stiffness remains positive) over all cycles up to the maximum lateral displacement of 1.5 t_r and under all angles of applied rotation considered in this study, including the maximum rotation of 0.03 rad. A small variation in the lateral response under vertical pressures of 2 MPa and 6 MPa for Isolator 1 and Isolator 2 can also be observed in Fig. 8. Negligible difference in the hysteresis loops can be observed at 10 MPa and for Isolator 3 under all three pressures.

4.1. Effects of rotational deformation on lateral stiffness

Fig. 9 shows the effect of lateral displacement amplitude on the lateral stiffness (K_L) for the isolators considered in this study. The lateral stiffness is determined based on the peak response of lateral loads (F_L) and displacements (U) observed over each cycle, using the following relation

$$K_L = \frac{F_{L,max} - F_{L,min}}{U_{max} - U_{min}} \quad (1)$$

Under small lateral displacements and with no applied rotation, the isolator remains in complete contact with the upper and lower surfaces, resulting in a near linear response. However when rotational deformation is applied, the isolator may lose contact with the loading surfaces due to lift-off, which leads to a reduction in effective shear area, and as such a reduction in the effective lateral stiffness (see Fig. 9). Since the probability of lift-off occurring is higher for isolators with a high aspect ratio [19], the reduction in lateral stiffness is significant for Isolator 1, and negligible for Isolator 3 as shown in Fig. 9. Under larger lateral displacements rollover occurs in all isolators leading to a reduction in the loaded shear area. The ability of U-FREI to rollover is a consequence of the unbonded application and the negligible flexural rigidity of the fiber reinforcement. With the introduction of rotational deformation and subsequent lift-off a nonlinear decrease in the effective lateral stiffness is observed to occur. According to Fig. 9, the difference in lateral stiffness under large lateral displacements is reduced. This implies that under larger lateral displacements the effect of loss in contact area due to rollover is much more significant than the loss of contact due to lift-off. As a result it can be concluded that the effect of rotational deformation on the effective lateral stiffness is negligible under larger lateral displacements for the isolators investigated. Finally, as the lateral displacement is further increased, the initially vertical sides of the isolator begin to make contact with the upper and lower loading surfaces (see Fig. 2a), resulting in a stiffening in the lateral response.

The effective lateral stiffness of the isolators is found to decrease as the applied lateral displacement is increased due to the reduction in the effective shear area. It is worth noting that

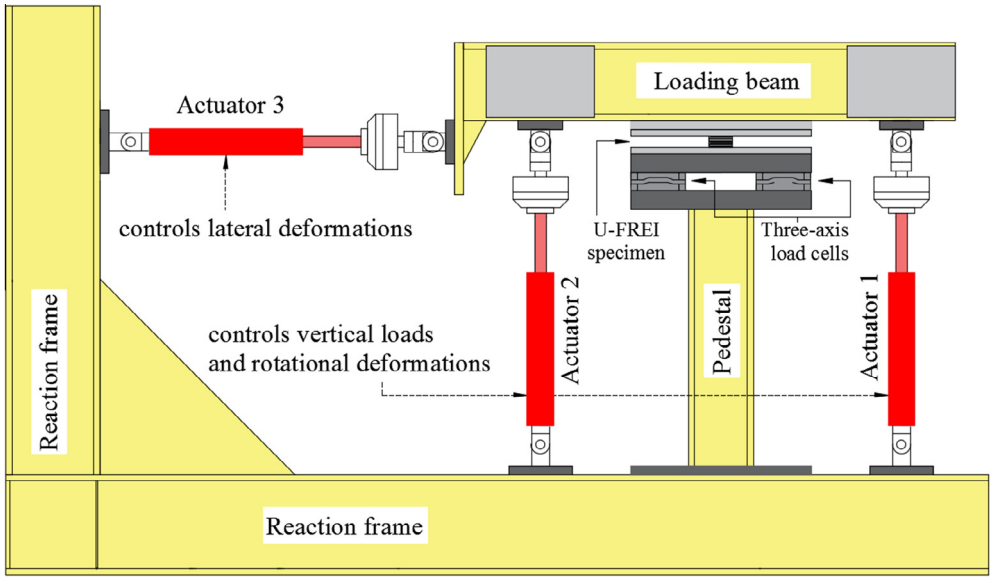

Fig. 6. Schematic of the three-degree of freedom test apparatus.

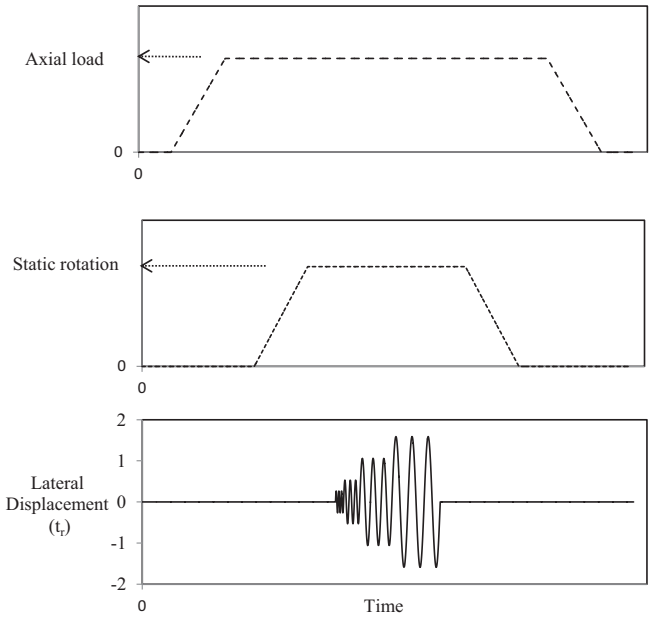

Fig. 7. The input signal time history.

the aforementioned behaviour of reduction in effective lateral stiffness as the applied lateral displacement increased is considered beneficial during the occurrence of earthquakes, particularly moderate (design) earthquakes [23], since a reduction in lateral stiffness results in an increase in the isolated period of the structure. This is expected to improve isolation efficiency as it further shifts in the structure's fundamental period away from the predominant periods associate with earthquakes. Additionally, the displacement demand on the isolator is limited by the stiffening response at larger lateral displacements as the effective lateral stiffness increases due to the initiation of contact between the supports and originally vertical faces of the isolator. In general, the effective lateral stiffness also reduces as the applied vertical load and angle of rotation are increased, particularly for isolators with lower aspect ratio values (see Fig. 9). Furthermore, it has been shown by Al-Anany et al. [24] that the vertical stiffness of the isolator can be maintained even under higher values of lateral offsets up to 1.50 t_r.

Table. 2 lists the corresponding isolated periods of the tested isolators using the effective lateral stiffness values determined from the third cycle, based on the following equation

$$T = 2\pi\sqrt{\frac{P/g}{K_L}} \tag{2}$$

where g is the gravitational acceleration. As previously mentioned, the lateral stiffness of U-FREI, which directly influences the time period, is primarily dependent on the amplitude of lateral displacement and applied vertical load. Accordingly, for the isolators investigated in this study the isolated periods are found to range between 0.40 and 1.45 s. This corresponds to full-scale isolated periods of 0.80–2.90 s (i.e. scale factor of 2.0). As a large number of bridges have a fundamental period in the range of 0.2–1.0 s [25], using the U-FREI considered in this study for the isolation of bridges could lead to a sufficiently large shift in the fundamental period that would result in a sizeable reduction in the seismic accelerations and forces on the bridges [1,26].

4.2. Effects of rotational deformation on lateral damping

Results presented in Fig. 10 show the influence of lateral displacement amplitude on the lateral damping of the isolators. The lateral damping was determined based on the area within the hysteresis loop (W_D), using the following equation

$$\zeta_L = \frac{2}{\pi}\left[\frac{W_D}{K_L(|U_{max}| + |U_{min}|)^2}\right] \tag{3}$$

As shown, the lateral damping was found to range from a minimum value of 7.5% to a maximum value of 13%, 14%, and 16% for Isolator 1, 2, and 3, respectively, which implies an increase in lateral damping with a reduction of the isolator aspect ratio. Additionally, an increase in the applied angle of rotation and vertical load were found to increase the lateral damping. A sufficient level of energy dissipation (damping) is needed in order to control isolator displacement amplitude. The advantage of damping in reducing isolator displacement is significant in bridges, where large displacements can lead to damage of the expansion joints [26]. Therefore, in addition to the ability of the U-FREI considered in this study to provide adequate seismic isolation periods, they are also able to produce sufficient damping to limit displacement demands.

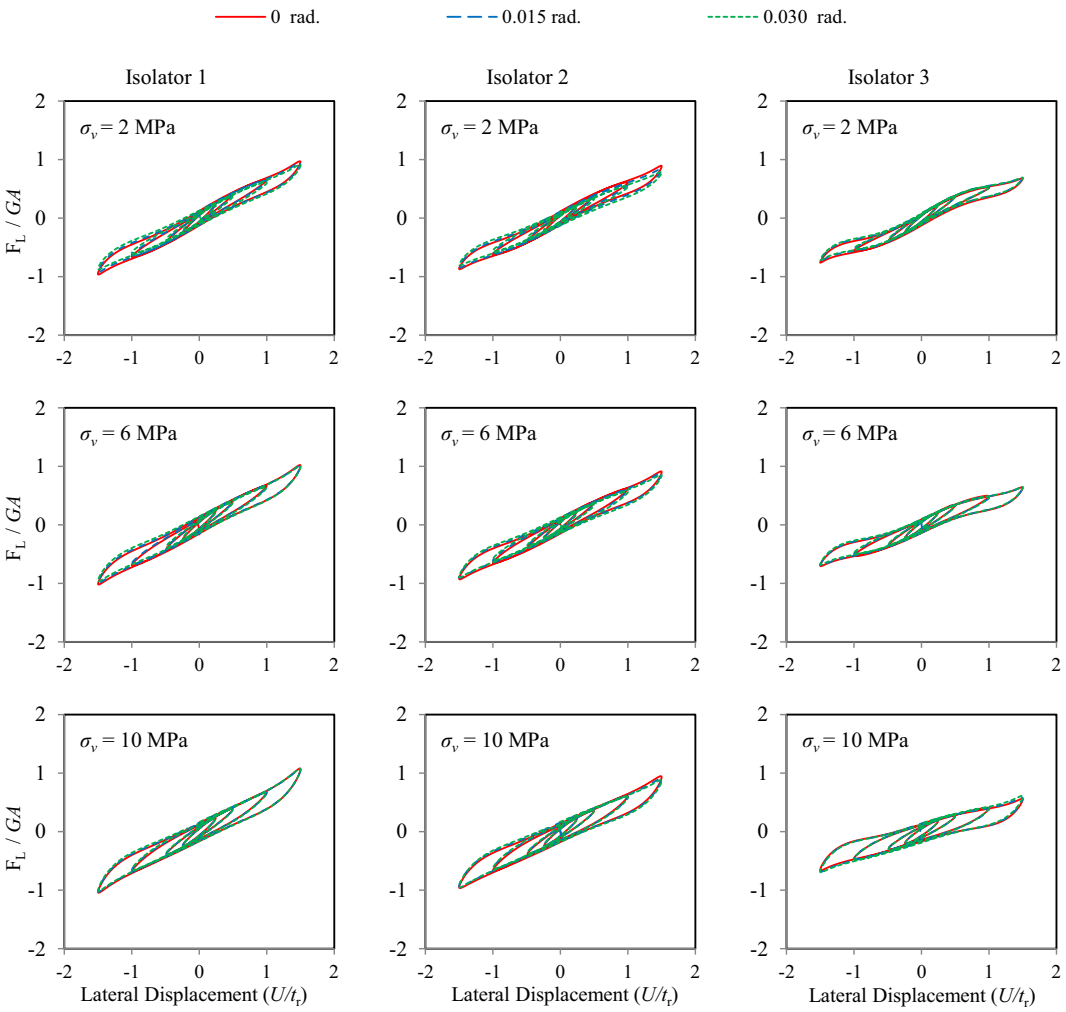

Fig. 8. Lateral hysteresis loops.

5. Finite element modelling

5.1. Model description and evaluation

Three-dimensional finite element (FE) modelling of the experimentally tested isolators was completed using the commercially available general-purpose program MSC Marc [27]. The FE analysis was employed in order to analyze the isolators under the critical loads/deformations considered during the experimental program. The primary objective of the FE study was to evaluate and assess the resulting stress and strain state in the isolators when subjected to the largest vertical loads (i.e. 10 MPa), rotational deformations (i.e. 0.03 rad), and lateral deformation (i.e. 1.5 t_r) considered in the experimental program.

The elastomer was represented by an eight-node isoparametric quadrilateral brick element (element type 74) with dimensions of 1.50 mm × 1.50 mm × 0.75 mm. The elastomer material was represented by a simplified single-parameter Mooney-Rivlin material model (i.e. Neo-Hookean). This hyperelastic model considers the elastomer compressibility and is defined by two parameters: the shear modulus, G_e, and bulk modulus, K_e. A membrane element with zero flexural rigidity and with linear elastic isotropic material properties was used to represent the fiber reinforcement, which was assumed to have zero flexural rigidity. The linear model employed for the fiber reinforcement is defined by two constants: the elastic modulus, E_f, and Poisson's ratio, υ_f. The material properties considered for modelling the isolators are listed in Table 3. While the value representing the fiber reinforcement elastic modulus, E_f, of 23 GPa was selected based on uniaxial tensile tests results.

The top and bottom loading supports were modelled as rigid surfaces. A rigid surface in MSC Marc is controlled in the vertical and lateral direction via a single node. However, in order to apply a rotation to this rigid surface an auxiliary node, which has a single rotational degree of freedom, must be defined. In this study the auxiliary node was only defined for the upper surface. As such, the upper rigid surface had three degrees of freedom (vertical, rotational, and lateral directions), while the bottom rigid surface was completely restrained from any movement. The loading procedure via FEM was identical to the experimental testing. The specimens were first loaded vertically to the desired loading level, and then rotational deformation was imposed before being laterally displaced. The unbonded contact between the isolators and the loading supports were simulated using the "Touching" contact model, which allows the nodal points at the top and bottom of the cover layers of the elastomer that are in contact with the supports to detach under sufficiently large lateral and rotational deformations when no normal compression stress exists. Accordingly, the shear forces along the contact interface between the isolator and the supports were transferred through a Coulomb friction mechanism.

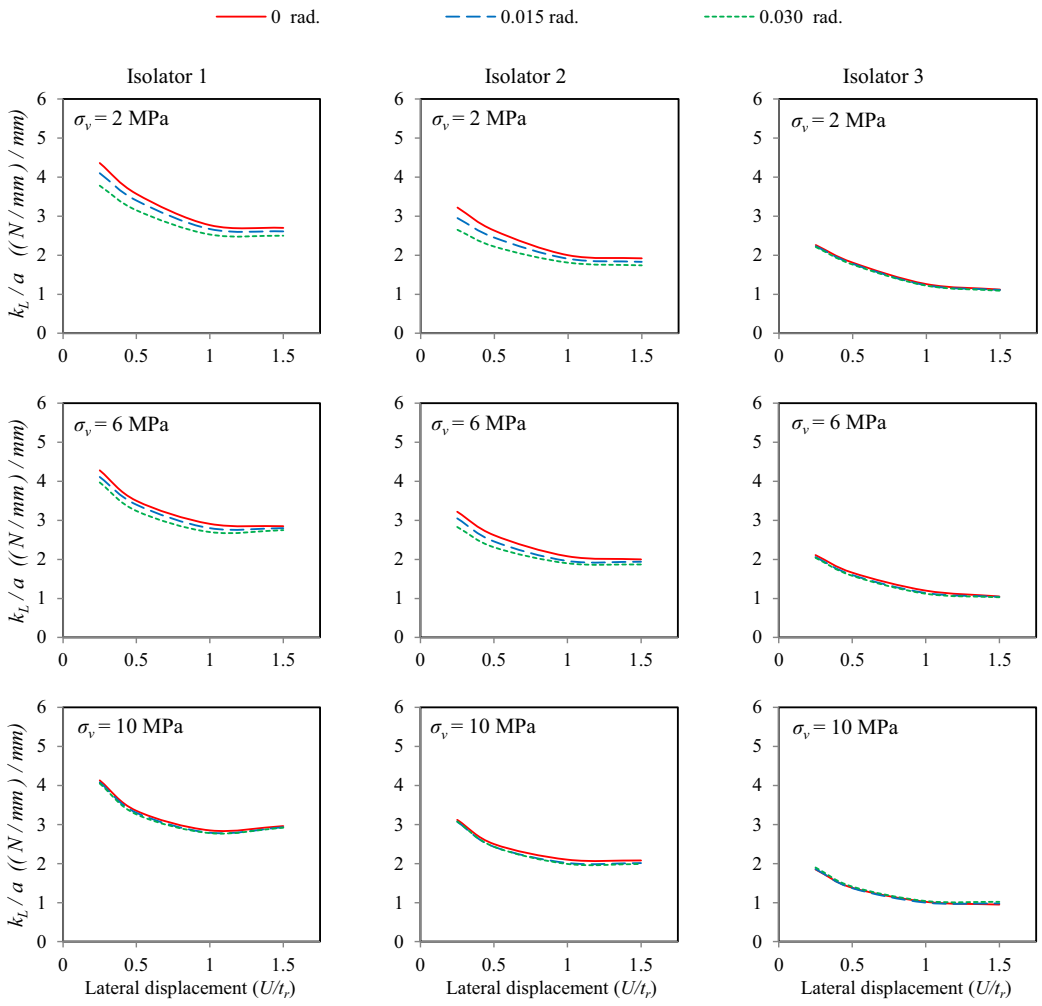

Fig. 9. Variation in lateral stiffness (K_L) for all isolators.

Table 2
Fundamental isolated period for the ¼ scaled isolators in seconds.

		σ_v = 2 MPa			σ_v = 6 MPa			σ_v = 10 MPa		
Isolator 1										
θ (rad.)=		0	0.015	0.03	0	0.015	0.03	0	0.015	0.03
U/t_r	0.25	0.40	0.42	0.43	0.70	0.72	0.73	0.92	0.93	0.93
	0.50	0.44	0.46	0.47	0.78	0.79	0.81	1.03	1.03	1.04
	1.00	0.50	0.51	0.53	0.85	0.87	0.89	1.11	1.13	1.13
	1.50	0.51	0.52	0.53	0.86	0.87	0.88	1.09	1.10	1.10
Isolator 2										
θ (rad.)=		0	0.015	0.03	0	0.015	0.03	0	0.015	0.03
U/t_r	0.25	0.41	0.43	0.46	0.72	0.74	0.76	0.94	0.95	0.94
	0.50	0.46	0.47	0.50	0.79	0.82	0.84	1.05	1.06	1.06
	1.00	0.52	0.54	0.55	0.89	0.92	0.93	1.14	1.17	1.17
	1.50	0.53	0.55	0.56	0.91	0.92	0.94	1.15	1.17	1.17
Isolator 3										
θ (rad.) =		0	0.015	0.03	0	0.015	0.03	0	0.015	0.03
U/t_r	0.25	0.42	0.42	0.42	0.75	0.76	0.76	1.03	1.03	1.02
	0.50	0.47	0.47	0.47	0.84	0.86	0.86	1.19	1.20	1.18
	1.00	0.56	0.56	0.57	0.99	1.02	1.03	1.39	1.40	1.37
	1.50	0.59	0.59	0.60	1.06	1.06	1.07	1.45	1.41	1.39

The friction coefficient was selected to be equal to one in order to prevent any slippage.

Table 4 compares the lateral stiffness of the isolators obtained from the experimental with the FE modelling results. Although the presented FE model considered a constant value for the shear modulus of the elastomer, which is characterized by strain dependency, the FE modelling provided a reasonable estimate to the lateral stiffness values over the entire range of lateral displacements with the error ranging between approximately -3% and 9%. In addition, Fig. 11 shows that the lateral response trend from the FE model is

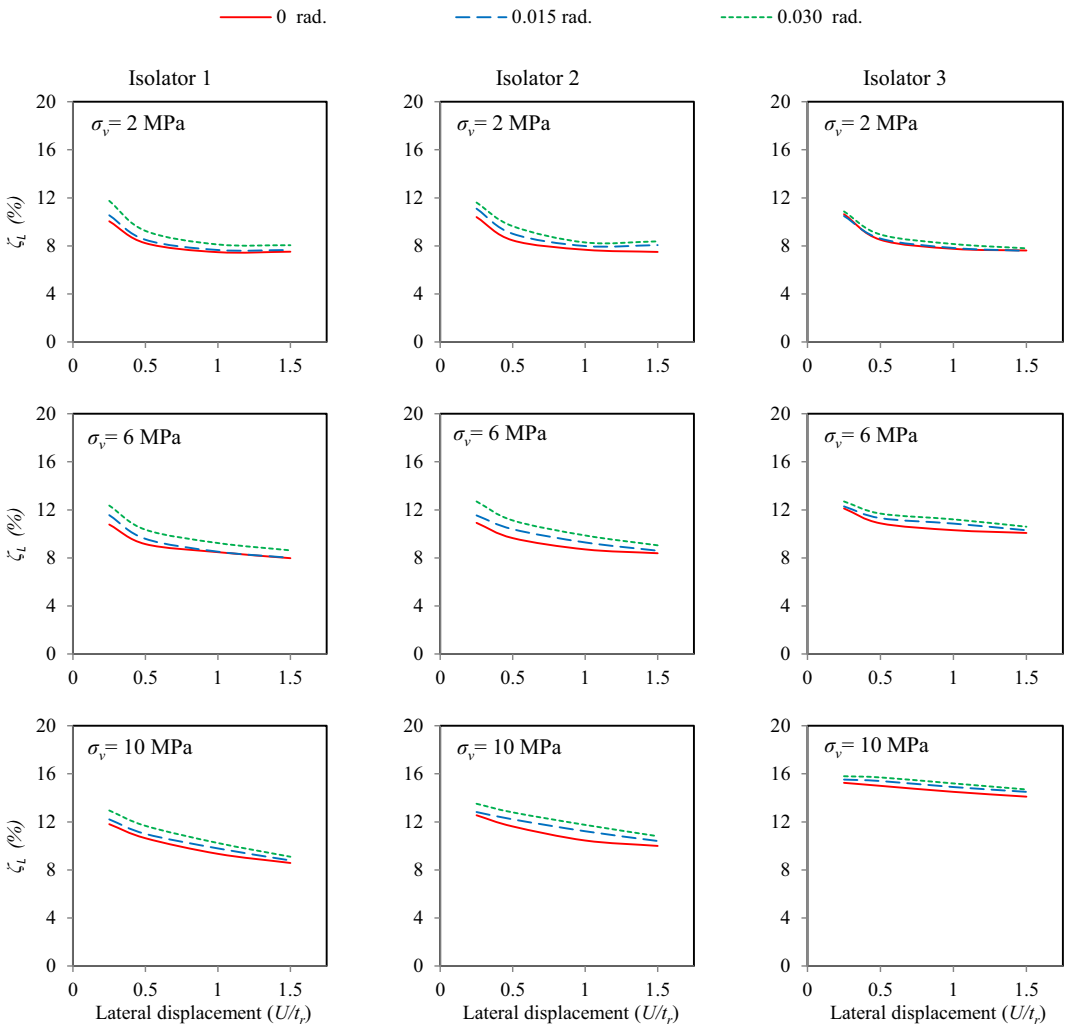

Fig. 10. Variation in isolator lateral damping (ζ_L).

Table 3
Material properties of the modeled isolators.

Elastomer material	Fiber material
Shear modulus (G) = 0.86 MPa Bulk modulus (K) = 2000 MPa	Elastic modulus (E) = 23 GPa Poisson's ratio (υ) = 0.20

in a good agreement with the experimentally measured loops. This level of agreement provides confidence in the accuracy of the presented model and its ability to capture the isolator lateral response.

6. Results and discussions of FE modelling

This section investigates the resulting normal stresses (σ_{11}, σ_{22}, and σ_{33}) and shear strain (γ_{12}) that develop in the three isolators. The stresses monitored are those generated according to the local axis of the elastomer layer (see Fig. 12), rather than the global axis. Additionally, the 3D analyses were completed using the Updated Lagrangian (UL) formulation, which allows the deformed configuration at the last completed increment to be the reference for the current configuration.

6.1. Normal stresses σ_{11}, σ_{22}, and σ_{33}

This section investigates the normal stresses that develop within the isolator as it is subjected to vertical, rotational and lateral deformations. Accordingly, the stresses are presented at four different phases. Phase I represents the deformation of the isolator under a mean compressive stress, σ_v of 10 MPa. Next, an angle of rotation equal to 0.03 rad is introduced in Phase II. Finally, Phase III and Phase IV represent the isolator under loading conditions of Phase I and Phase II, but when subjected to either a positive or

Table 4
Error in (%) for the calculated stiffness between the experimental and FEM results.

U/t_r	Exp.	FEM	Error (%)
Isolator 1			
0.25	4.05	3.84	5.2
0.5	3.26	3.25	0.3
1	2.78	2.86	−3
1.5	2.92	2.88	1.3
Isolator 2			
0.25	3.08	2.9	5.8
0.5	2.43	2.42	0.5
1	1.99	2.04	−2.6
1.5	1.99	1.94	2.7
Isolator 3			
0.25	1.9	1.74	8.6
0.5	1.41	1.38	2.1
1	1.04	1.04	−0.3
1.5	1.02	0.93	9.2

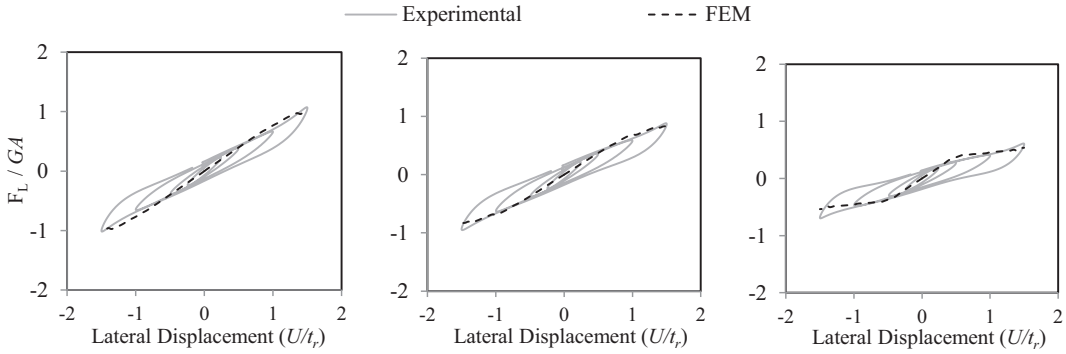

Fig. 11. Comparison of the numerically obtained lateral response of the U-FREI with the experimental response.

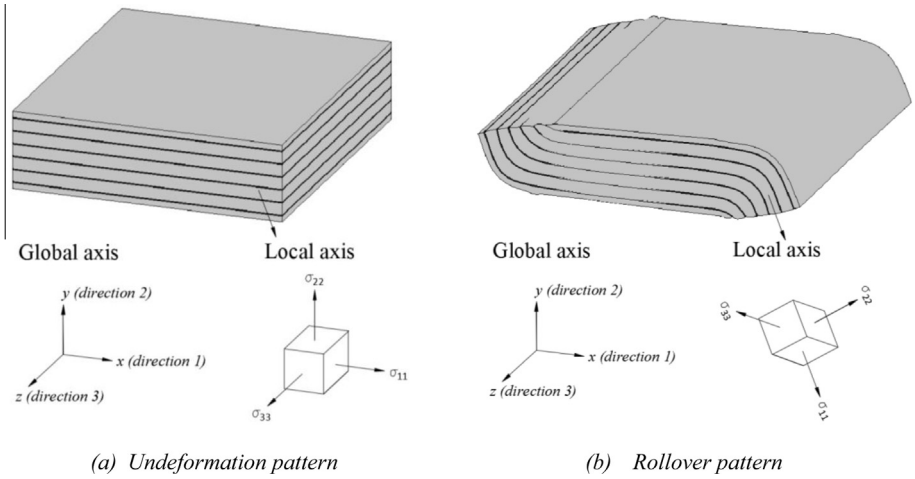

(a) Undeformation pattern *(b) Rollover pattern*

Fig. 12. Definition of Stresses.

negative lateral deformation of 1.5 t_r. These four phases represent the maximum deformation experienced by the isolators in this study.

Figs. 13–15 presents the contours of normalized normal stresses σ_{11}, σ_{22}, and σ_{33}, developed within Isolator 1, 2, and 3, respectively, during the four phases considered. The three orthogonal stresses have been normalized with respect to the mean vertical stress σ_v and only half of the isolator is shown. It can be observed that the difference in distribution and peak values of the normalized stresses in the three considered orthogonal directions in a particular isolator is negligible. This observation confirms that the hydrostatic rule can be used to define the pressure distribution in the isolators under the considered deformation.

As seen in Figs. 13–15, an applied angle of rotation leads to an increase of the normal stresses on the loaded side of the isolator due to a reduction in the size of the loaded area. However, insignificant tensile stresses are found to occur on the unloaded side of the isolator due to the detachment of the isolator from the contact supports. Additionally, the rate of increase in the peak stresses under different patterns of deformation is a factor of the isolator aspect ratio and also the ratio of plan dimensions of the isolator (i.e. ratio of length, *2b*, to width, *a*). As an example, under a mean vertical stress of 10 MPa (i.e. Phase I), the peak normalized value of stresses for Isolator 2 with a plan dimension ratio of 0.89 (i.e. rectangular) and Isolator 3 with a plan dimension ratio of 0.35 (i.e. longer strip) is equal to 1.90 and 1.70, respectively. This trend is in agreement with the theoretical solutions for predicting the stress values [28]. Additionally, the increase in the peak value of normal stresses due to the application of rotational deformation was approximately 28.9%, 13.2%, and 2.9% for Isolator 1 and 2, and 3, respectively. This is due to the fact that the decrease in the isolator aspect ratio results in an increase in the isolator flexibility and thus its ability to accommodate the applied rotation without lift-off (i.e. losing contact area). However, under lateral deformation, the reduction in the contact area becomes more evident for isolators with lower aspect ratios. For instance, the increase in the peak value of normal stresses in the rotated isolators under lateral deformation was found to be approximately 6.1%, 11.6%, and 22.8% for Isolator 1 and 2, and 3, respectively.

6.2. Shear strain γ_{12}

A primary cause of failure in bridge bearings/isolators has been reported to be due to shear delamination of reinforcement from the elastomer layers [21]. Consequently, bridge design codes, such as the *Canadian highway bridge design code* (CHBDC) CAN/CSA-S6-14 (CSA 2014) [29] and the *LRFD bridge design specifications* (AASHTO 2012) [30], specify a limit on the sum of the shear strains that developed within the isolator under vertical, rotational, and lateral deformation.

Fig. 16 presents the shear strain γ_{12} contours at the center of isolators for Phase I through Phase VI. It can be observed that the orientation of the peak shear strain varies according to the loading condition applied on the isolator. Under pure vertical deformation, the peak shear strains are observed to occur at the edges of the elastomer layers (i.e. x = ±b), however, under rotational deformation, the peak values continue to increase at the edge location, but on the loaded side of the isolator. Finally, it should be

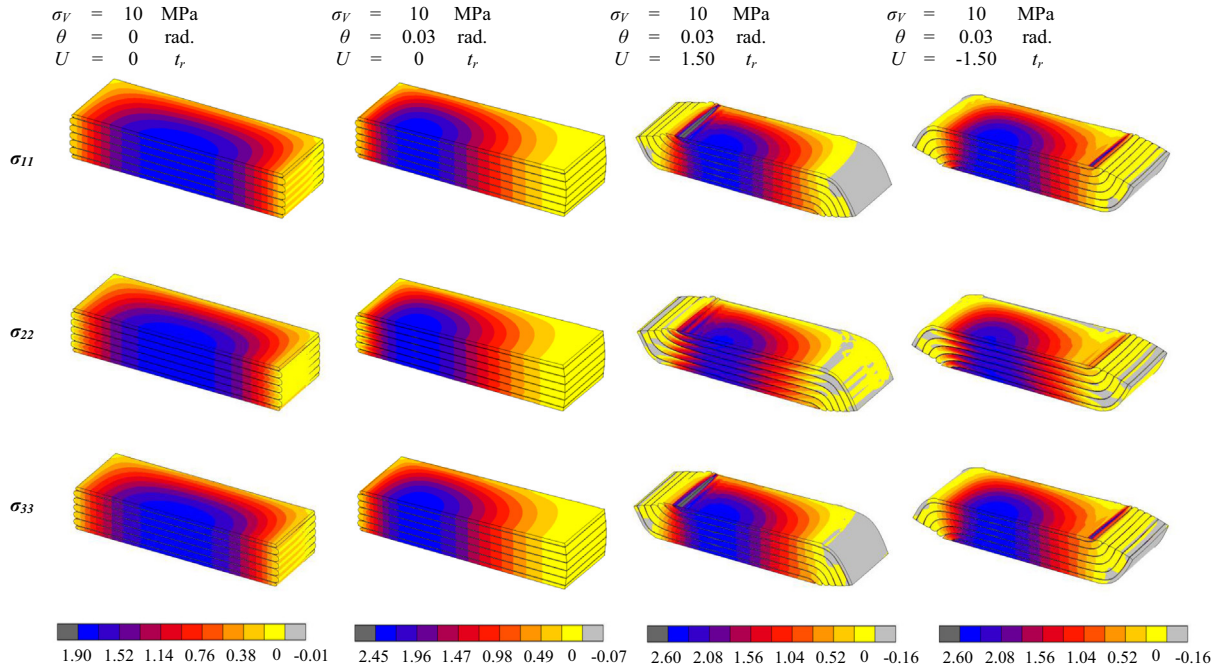

Fig. 13. Contours of normalized stresses (σ / σ_V) in *Isolator 1*.

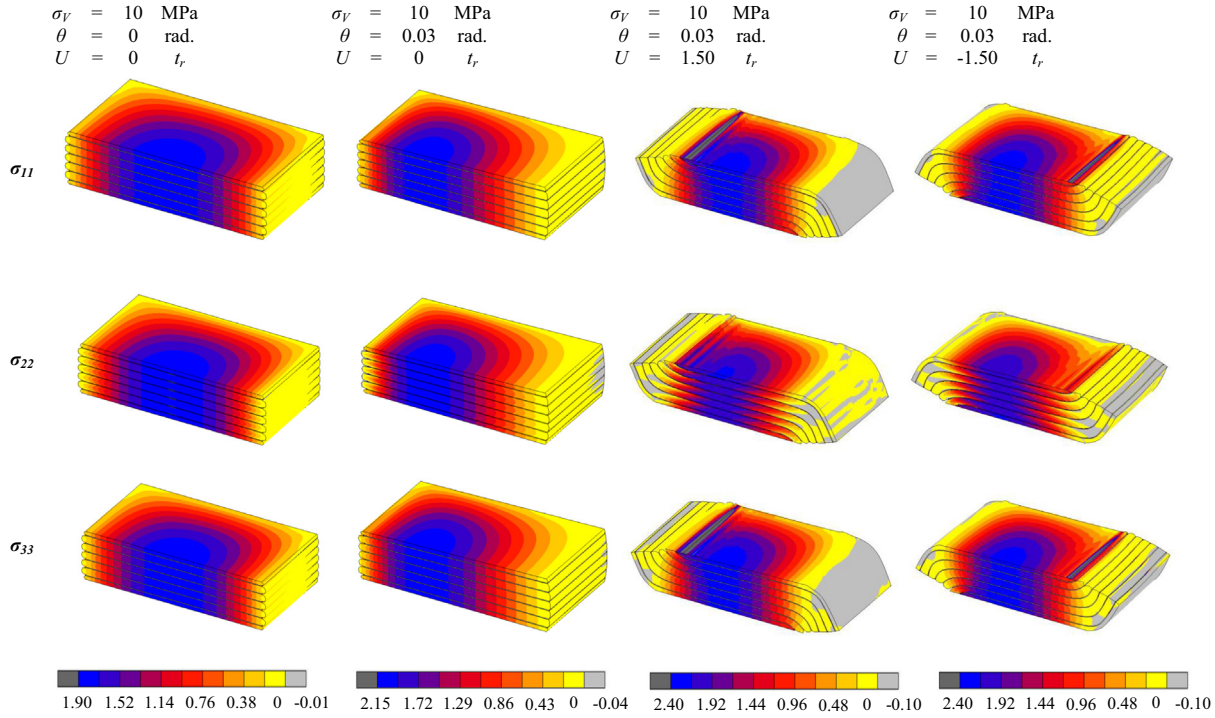

Fig. 14. Contours of normalized stresses (σ / σ_V) in *Isolator 2*.

noted that under lateral deformation, shear strains with higher values are localized at the corner of the top and bottom elastomer layers in the contact zone between the isolator and the loading plate.

7. Conclusions

This research paper investigates the effect of coupled vertical-rotational deformation on the lateral response of unbonded Fiber-Reinforced Elastomeric Isolators (U-FREI). The investigation was carried out experimentally using a 3 DOF test apparatus and numerically using the commercially available finite element software MSC Marc [27]. The test apparatus employed for the experimental testing was designed to apply deformations in three different directions (i.e. vertical, rotational, and lateral) independently and/or in combination. Thus, it was able to conduct different loading conditions on the isolators expected during the lifetime of a bridge. The novelty of the experimental testing was based on the ability to include the effect of the rotational deformation, which is

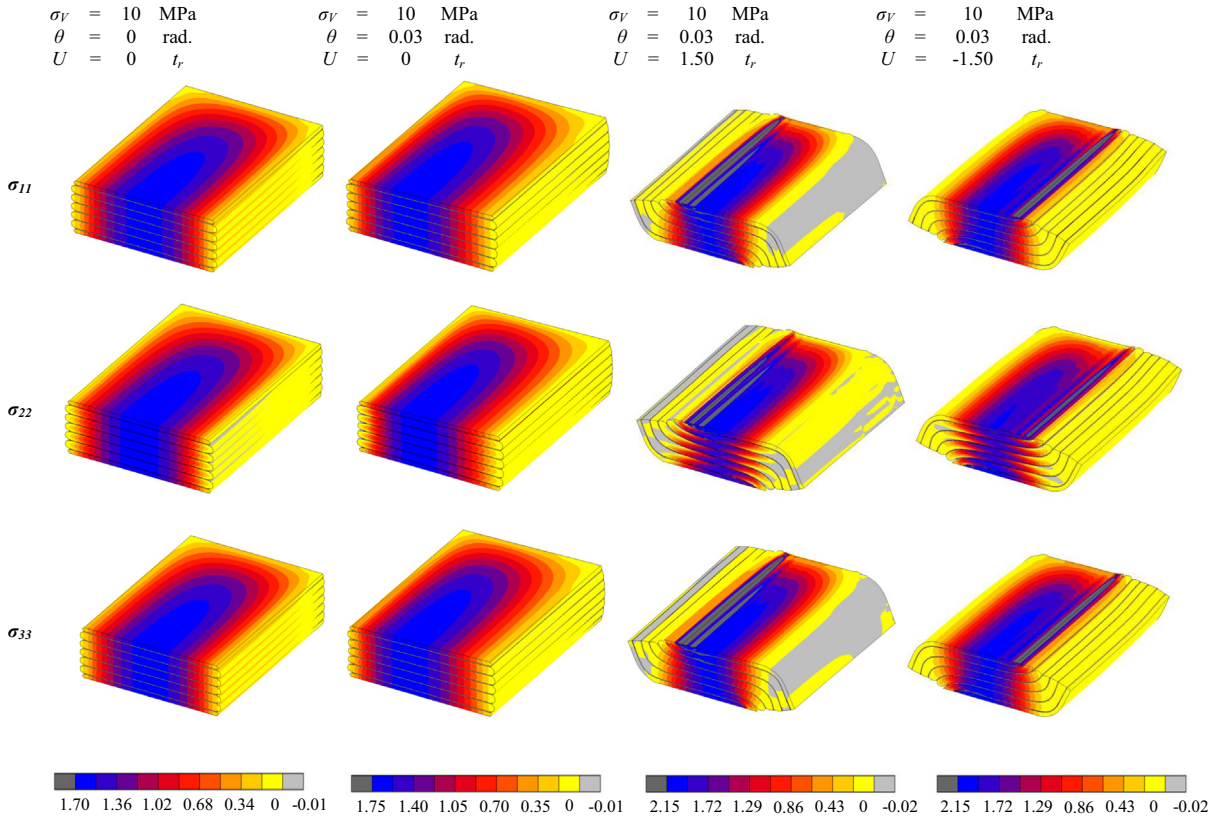

Fig. 15. Contours of normalized stresses (σ / σ_V) in *Isolator 3*.

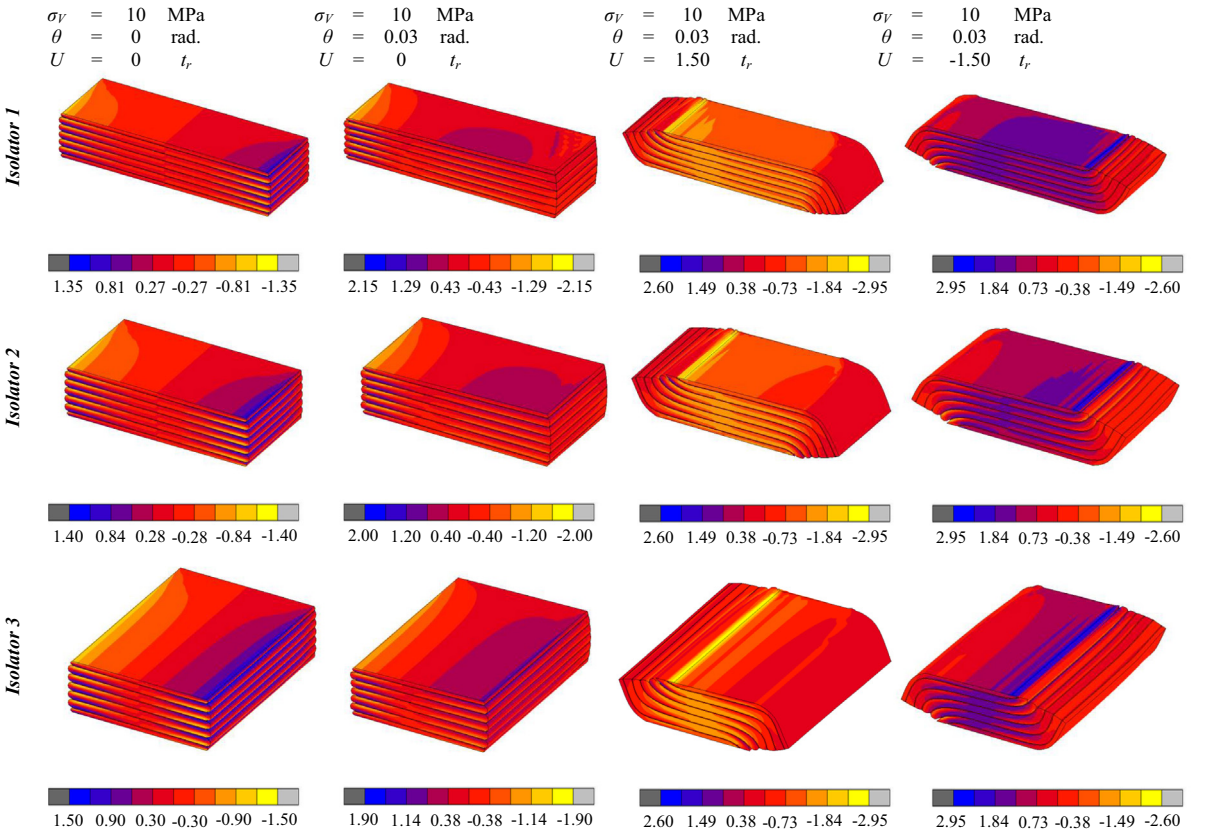

Fig. 16. Contours of shear strain (γ_{12}).

considered an important aspect in bridge bearings/isolators design, on the lateral response of the isolators. Additionally, three-dimensional finite element modelling was performed on the isolators in order to evaluate the stresses and strains that develop under the peak applied load and deformations. The three isolators considered in this study had in-plane aspect ratios of 2.5, 2.5, and 4.5, but a constant shape factor of 6.0 was maintained.

The main findings from the experimental study are:

1. A rotational deformation up to 0.03 rad had a negligible effect on the lateral response of all isolators in general, but was with the least significant for isolators with lower aspect ratios.
2. Increasing both the applied vertical load as well as the angle of rotation on the isolator caused a slight decrease in the lateral stiffness and small increase in the lateral damping.
3. The isolation periods of the considered isolators varied according to the values of the applied vertical loads and angle or rotation, with a maximum calculated value of approximately 2.90 s.

Based on results from FEM the following main conclusions were drawn:

1. The hydrostatic rule can be used to define the distribution of pressures that are developed within the elastomeric isolators, not only vertical deformation, but also if under coupled vertical-lateral-rotational deformation.
2. Decreasing the aspect ratio of the isolator delay the occurrence of lift-off, this results in a lower rate of increase in the normal stresses and shear strains under rotational deformation. However, it also results in a larger rate of increase in stresses and strains developed within the isolator when subjected to lateral deformations.

Acknowledgements

This research was carried out as part of the mandate of the Centre for Effective Design of Structures (CEDS) at McMaster University. The support of the Natural Sciences and Engineering Research Council of Canada (NSERC) and the Ontario Ministry of Research and Innovation (MRI) is gratefully acknowledged.

References

[1] Jangid R. Seismic response of isolated bridges. J Bridge Eng 2004;9(2):156–66.
[2] Naeim F, Kelly J. Design of seismic isolated structures: from theory to practice. New York: John Wiley & Sons Inc.; 1999.
[3] Caltrans. Bridge Memo to Designers. Section 7: Bridge Bearings. California Department of Transportation, Sacramento, California; 1994.
[4] Konstantinidis D, Kelly J, Makris N. Experimental investigations on the seismic response of bridge bearings. Report No. EERC-2008/02, Earthquake Engineering Research Center, University of California, Berkeley; 2008.
[5] Kunde M, Jangid R. Effects of pier and deck flexibility on the seismic response of isolated bridges. ASCE J Bridge Eng 2006;11(1):109–21.
[6] Girish M, Pranesh M. Sliding isolation systems: state-of-the-art review. IOSR J Mech Civil Eng 2013;6:30–5 (IOSR-JMCE) 02/2013.
[7] Tsopelas P, Constantinou M, Kim Y, Okamota S. Experimental study of FPS system in bridge seismic isolation. Earthquake Eng Struct Dynam 1996;25(1):65–78.
[8] Tsopelas P, Constantinou M, Okamota S, Fujii S, Ozaki D. Seismic performance of highway bridges. Eng Struct 1996;18(4):301–10.
[9] Ghobarah A, Ali H. Seismic performance of highway bridges. Eng Struct 1988;10(3):157–66.
[10] Wesolowsky M, Wilson J. Seismic isolation of cable-stayed bridges for near-field ground motions. Earthquake Eng Struct Dynam 2003;32:2107–26.
[11] Matsagar V, Jangid R. Seismic response of simply supported base-isolated bridge with different isolators. Int J Appl Sci Eng 2006;4(1):53–69.
[12] Konstantinidis D, Kelly J. Two low-cost seismic isolation systems. In: 15th world conference on earthquake engineering. Lisbon, Portugal, September 24–28; 2012.
[13] Toopchi-Nezhad H, Tait M, Drysdale R. Testing and modeling of square carbon fiber-reinforced elastomeric seismic isolators. Struct Control Health Monit 2008;15(6):876–900.
[14] Toopchi-Nezhad H, Tait M, Drysdale R. Lateral response evaluation of fiber-reinforced neoprene seismic isolators utilized in an unbonded application. ASCE J Struct Eng 2008;134(10):1627–37.
[15] Toopchi-Nezhad H, Drysdale R, Tait M. Parametric study on the response of stable unbonded fiber-reinforced elastomeric isolators (SU-FREIs). J Compos Mater 2009;43(15):1569–87.
[16] Toopchi-Nezhad H, Tait M, Drysdale R. Shake table study on an ordinary low-rise building seismically isolated with SU-FREIs (stable unbonded fiber-reinforced elastomeric isolators). Earthquake Eng Struct Dynam 2009;38(11):1335–57.
[17] Toopchi-Nezhad H, Tait M, Drysdale R. Bonded versus unbonded strip fiber reinforced elastomeric isolators: finite element analysis. Compos Struct 2011;93(2):850–9.
[18] Al-Anany Y, Tait M. A study on the rotational behaviour of bonded and unbonded fiber reinforced elastomeric isolators. In: 11th Canadian Conference on Earthquake Engineering, Victoria, British Columbia, Canada, 21–24 July 2015.
[19] Al-Anany Y, Tait M. A numerical study on the compressive and rotational behavior of fiber reinforced elastomeric isolators (FREI). Compos Struct 2015;133:1249–66.
[20] Al-Anany Y, Tait M. Experimental assessment of fiber-reinforced elastomeric isolators for bridge applications. Compos Part B: Eng 2016. under review.
[21] Van Engelen N, Tait M, Konstantinidis D. Model of the shear behavior of unbonded fiber-reinforced elastomeric isolators. ASCE J Bridge Struct Eng 2014;141(7):04014169.
[22] Stanton J, Roeder C, Mackenzie-Helnwein P, White C, Kuester C, Craig B. Rotation limits for elastomeric bearings. Report No. NCHRP 596, Transportation Research Board, National Cooperative Highway Research Program, Washington, D.C.; 2007.
[23] Foster B. Base isolation using stable unbonded fibre reinforced elastomeric isolators (SU-FREI) Master's thesis. Hamilton: McMaster University; 2011.
[24] Al-Anany Y, Van Engelen N, Tait M. Experimental investigation on the vertical and lateral behaviour of unbonded fiber-reinforced elastomeric isolators. Compos Constr 2016. under review.
[25] Kunde M, Jangid R. Seismic behavior of isolated bridges: a-state-of-the-art review. Electron J Struct Eng 2003;3(2):140–69.
[26] Constantinou M, Kalpakidis I, Filiatrault A, Ecker Lay R, LRFD-based analysis and design procedures for bridge bearings and seismic isolators. Report No. MCEER-11-0004, Multidisciplinary Center for Earthquake Engineering Research, University at Buffalo, State University of New York, Buffalo, New York; 2011.
[27] MSC, Marc. Santa Ana, CA: MSC Software Corporation; 2013.
[28] Tsai H, Kelly J. Stiffness analysis of fiber-reinforced elastomeric isolators. Pacific Earthquake Engineering Research Center, PEER, Berkeley, California; 2001/5.
[29] CSA, Canadian highway bridge design code, Standard CAN/CSA-S6-14, Canadian Standards Association International, Ontario; 2014.
[30] AASHTO, LRFD bridge design specifications, American association of state highway and transportation officials, Washington, DC; 2012.